2025 IEEE International Symposium on Circuits and Systems (ISCAS) | 979-8-3503-5683-0/25/$31.00 ©2025 IEEE | DOI: 10.1109/ISCAS56072.2025.11043572

A Transceiver for NMR Field Probes Integrated in a Low-Power CMOS Process

Guillaume Mocquard*, Oskar Bjorkqvist†, Klaas P. Pruessmann† and Thomas Burger*
*Integrated Systems Laboratory, ETH Zurich, Zurich, Switzerland
†Institute for Biomedical Engineering, ETH Zurich and University of Zurich, Zurich, Switzerland
Email: {mocquard, burger}@iis.ee.ethz.ch

***Abstract*—This paper presents a CMOS transceiver for field monitoring in magnetic resonance imaging (MRI) scanners. The integrated circuit (IC) is optimized for usage in magnetic field strengths of 3 T and 7 T. The transceiver integrates a transmitter capable of exciting a nuclear magnetic resonance (NMR) field probe up to a peak-to-peak voltage of 143 V thanks to a resonant tank. This NMR-on-a-chip also implements a low-IF quadrature receiver. The receiver, including transimpedance amplifiers (TIA) and measurement output buffers, consumes only 14.1 mW. The measured signals acquired in a full-body scanner result in an input-referred noise of 390 pV/$\sqrt{\text{Hz}}$ owing to a resonant network passively amplifying the probe signal to the low-noise amplifier (LNA) input. The overall transceiver is integrated into a 65 nm CMOS process covering a total area of 1.5 mm^2.**

***Index Terms*—Magnetometer, MRI, NMR, NMR-on-a-chip, transceiver**

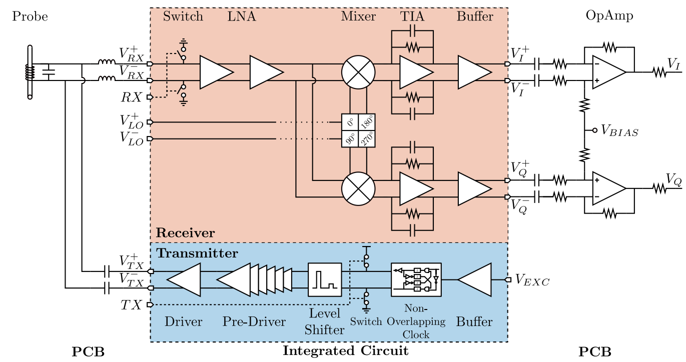

Fig. 1. General architecture of the designed ASIC and its immediate surroundings represented in receive mode

I. Introduction

Magnetic Resonance Imaging (MRI) is one of the most widely used imaging technologies with diverse applications in clinical diagnostics, medical research, and the life sciences. The quality of MR images depends on the accuracy of intricate magnetic field dynamics used for signal encoding. One strategy for improving MRI is thus to measure field dynamics during scans and account for their imperfections at the level of image reconstruction [1]. High field sensitivity and temporal resolution for this purpose can be achieved with probes based on nuclear magnetic resonance (NMR), i.e., on the same physical effect as underlies MRI itself [2]–[4].

Tight space in MRI systems, proximity to the patient, and variable imaging setups call for small, movable NMR probes with local, low-power electronics. Related progress has recently been made in portable systems for NMR spectroscopy, deploying integrated transceivers to lower power requirements [5]–[7]. For large sensitive volumes and thus high power for excitation, a high-voltage process has been used [6]. Low input-referred noise has been achieved by taking advantage of the bipolar transistors of a SiGe BiCMOS process [7]. Recently, the use of transmit radiofrequency (RF) fields in MRI as a power source has been demonstrated without affecting image quality nor safety [8]. Moreover, an application-specific integrated circuit (ASIC) achieving phase synchronization and creating triggering events for wireless sensors has been presented [9]. Towards autonomy of field probes, self-synchronization and self-calibration have recently been reported [10]. In light of these advances, integrated probe electronics with even lower power demands are called for.

This paper presents an integrated NMR transceiver (Fig. 1) for field probing, optimized for placement in MRI scanners with a magnetic field strength of 3 T and 7 T. Its novel resonant network architecture relaxes the specifications of the transmitter and the receiver, allowing for low-power architecture. Passive amplification from the transmitter permits a typical low-power CMOS process to reach a high excitation voltage at the probe coil. Passive amplification from the probe towards the receiver ensures low input-referred noise despite the use of typical CMOS transistors. Series protection switches, ordinarily used at the LNA input, are removed thanks to series inductors.

II. Implementation of the Magnetometer

The ASIC shown in Fig. 2 was designed and fabricated in a bulk 65 nm CMOS technology. The chip dimensions, including the pad ring structure, are 1.5 mm × 1 mm. The circuit implementation of the relevant building blocks is elaborated next.

A. Field Probe

The ASIC has been designed to be associated with an NMR field probe as the one used in [4]. In our case, the glass capillary (inner diameter 1.3 mm, outer diameter 1.7 mm) contains hexafluorobenzene. It uses the relaxation of fluorine (^{19}F), whose gyromagnetic ratio is slightly lower than that

This work was supported in part by the Swiss National Science Foundation (SNSF) [181023].

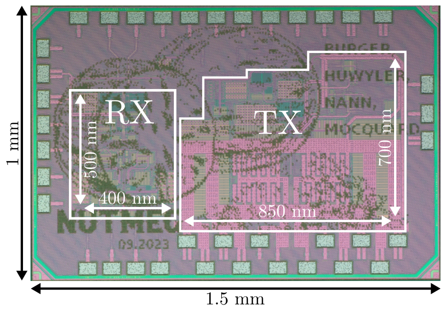

Fig. 2. Chip micrograph and main building blocks of the transceiver IC

of protons (^{1}H). This prevents unwanted NMR excitation by the MR scanner imaging protons. Enameled copper wire wound around the capillary forms a 5-turn solenoidal MR coil. The active sample volume is around 1 µL. An ellipsoidal epoxy casing surrounds the capillary to counter deviations in magnetic susceptibility, which otherwise would be detrimental to the NMR signal lifetime. The probe is connected to the transceiver IC on a Printed Circuit Board (PCB) via a resonant network consisting of capacitors and inductors as described in Fig. 1. Its inductance reaches 79 nH, considering the wiring to the PCB pads.

B. Resonant Network

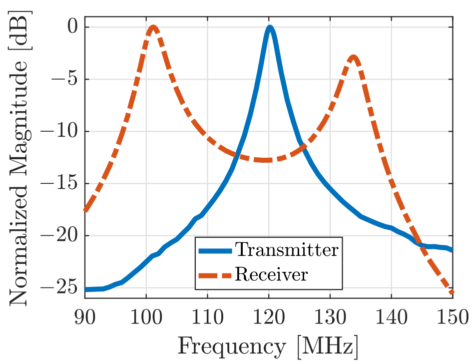

Fig. 3. Measured frequency response of the transceiver IC and its output network including a field probe in transmit and receive modes

Unlike previously designed front-end networks, the LC resonator presented in this paper and visible in Fig. 1 affords a passive amplification in both transmit and receive modes. The resonant network is adjusted depending on the desired field strength of the MRI scanner. The measured frequency response associated with the transceiver optimized for NMR of fluorine in a 3 T MRI scanner appears in Fig. 3. The parallel capacitors to the probe and the series one to the transmitter are tuned to center the resonance of the transmitter around the desired frequency of 120.15 MHz in the present case. The inherent gain of the network reduces the amplification needs of the transceiver. The transmitter can use a standard low-power CMOS process and generate enough current to excite the probe. The ratio between the capacitors results from a trade-off between the transmitter's passive amplification and the quality factor of the system, hence the Signal-to-Noise Ratio (SNR) on the receiver side. It consequently affects the excitation pulse duration. The series inductors at the receiver input are made as large as possible to produce a high passive amplification towards the LNA input while centering the plateau in the receiver's frequency response around the desired frequency. This choice ensures a constant passive amplification for all frequencies in the band of interest.

C. Transmitter

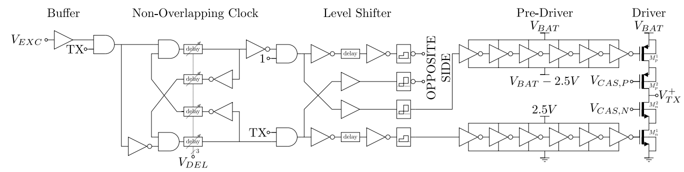

Fig. 4. Simplified circuit schematic of the transmitter with the pre-drivers and driver of the positive output only

Figure 4 displays the main blocks composing the transmitter. A high-voltage CMOS process is not necessary since the resonant network around the probe amplifies the transmitter output. The driver is a class-D power amplifier realized with I/O transistors. The absence of a resonator, the efficiency, and the possibility of extending the maximum tolerable voltage due to stacking are the reasons leading towards this architecture. The transceiver ASIC has been foreseen to integrate a battery-operated system. The voltage supply of a typical lithium-ion battery lying at 3.7 V exceeds the limit of 2.5 V for the I/O transistors in the technology used. Hence, the driver integrates cascode transistors to limit the voltage drop seen by each transistor. The total width of the NMOS and PMOS transistors reaches 3.5 mm and 5.5 mm, respectively. The high current being driven requires a high supply decoupling on-chip. High-density capacitors stacking MOS, MOM, and MIM capacitors implement close to 600 pF of capacitance for that purpose.

The high- and low-side pre-drivers are implemented with 2.5 V I/O transistors and hence necessitate the generation of different supplies. The low-side drivers require a supply of 2.5 V in addition to the ground. It is generated on-chip from the battery supply thanks to a conventional class-AB voltage buffer [11] with high output current sinking and sourcing capabilities. A classical five-transistor OTA in unity-gain buffer configuration precedes the class-AB buffer. The 2.5 V drop from the battery voltage necessary for the high-side pre-driver relies on a similar architecture.

Upstream of the aforementioned pre-drivers, level shifters translate the input from the core 1.2 V supply to different levels. A modified version of the conventional level shifter and a high-voltage (HV) tolerant level shifter realize this function as in [12]. Additional inverters placed beforehand ensure a proper delay propagation after voltage translation despite the HV tolerant level shifter requiring two stages.

A Non-Overlapping Clock (NOC) generation circuit realizes the low- and high-side control signals from a buffered input reference. An on-chip low-dropout (LDO) regulator supplies those circuits. Delay cells with buffered RC time constant adjust the non-overlap time, thus the amplitude at the transmitter output. Resistive transmission gates implement the resistance of the delay cells. Designed to accommodate 3 T and 7 T MRI scanners, an additional parallel transmission gate is switched in to adjust the delay when the excitation frequency lies around 280 MHz rather than 120 MHz. Switches at the output of the NOC short the control signals to the rails to ensure that the drivers do not consume any power in receive mode.

D. Receiver

Figure 1 introduces the main blocks of the receiver. Figure 5 presents the architecture of the LNA that consists of two AC-coupled class-AB inverter-based amplification stages with replica biasing. The AC-coupling allows for *n*- and *p*-side transistor g_m matching by appropriate coupling capacitor scaling and to keep the LNA input DC common-mode (CM) level at the ground using NMOS-only switches. The latter are closed during TX excitation to protect the LNA input and keep the signal swing bounded. Both stages feature cascodes to increase gain and isolation. The second stage uses resistive feedback for linearization and low input and output impedance such that the stage can drive the subsequent down-conversion mixer. The common-mode level of the LNA output at half the supply voltage is established over a CM feedback amplifier at the output of the 2nd stage. The LNA is generally broadband, limited by the AC coupling in the low MHz range on the low side and by the capacitive loading of the 2nd stage on the high side. The LNA is adapted to the specific magnetic resonance frequencies by choosing the input inductance and tuning the capacitor bank at its input.

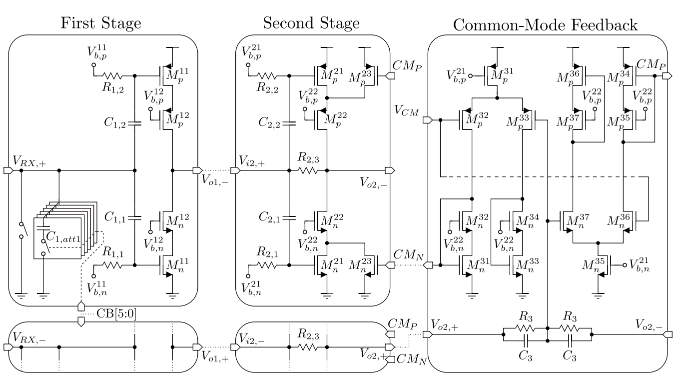

Fig. 5. Simplified circuit schematic of the two-stage LNA at the receiver input

A resistive input mixer converts the RF signal down to a low-IF I/Q receiver at 1 MHz where it is turned into voltage again with the help of a transimpedance amplifier (TIA). The choice of a 1 MHz intermediate frequency (IF) allows for high pass filtering around 100 kHz to avoid DC-offset issues, suppress the 1/f noise of the TIA, and cover well a signal bandwidth of 1 MHz to accommodate the typical field range in an MRI system. The mixer is operated with a 25 % duty cycle generated by a Windmill frequency divider [13] for improved noise performance and low power consumption. A third-order multi-path feed-forward architecture followed by a class AB output stage [14] realizes the TIA. It achieves a higher linearity, in-band gain, and bandwidth with a lower power consumption than a two-stage Miller-compensated architecture. The resistive and capacitive feedback of the TIA defines a low-pass filtering at 3 MHz.

The differential quadrature signals are then buffered and recombined into single-ended signals on board to minimize the cables required for the measurement.

III. Electrical Characterization

A custom board interfaces the packaged IC with the laboratory equipment. An nRF52840 from Nordic Semiconductor communicates with the ASIC to set the internal registers via a serial peripheral interface (SPI).

A. Transmitter

A fraction of the signal around the NMR probe was measured thanks to a capacitive voltage divider via the addition of capacitors connected to the NMR probe's pads on the PCB. A low capacitance ensures a minimum loading of the resonant network plus a reasonable dividing factor when a low-inductive passive oscilloscope probe is connected. The combination of a 1 pF capacitance with a 9.5 pF oscilloscope probe leads to a divider ratio of 10.5.

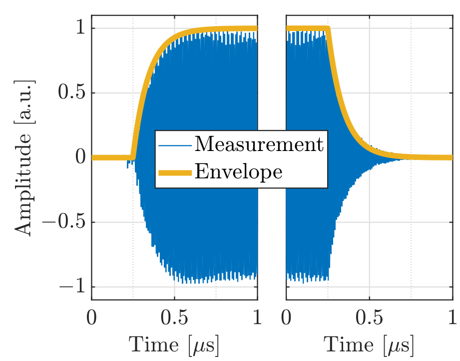

Fig. 6. Measured transient waveform around the field probe in transmit mode during the startup and shutdown phases. The 120.15 MHz excitation signal is sampled at 1 GHz.

Due to the resonant network around the field probe, the startup and shutdown operations are not instantaneous but exhibit exponential growth and decay, as seen in Fig. 6. The time constant depends on the quality factor of the outside components and on the conduction and wiring losses of the TX driver. The envelope reaches its maximum in about 250 ns. Therefore, the front-end permits the excitation of the probe with a pulse duration of a few microseconds without having an unacceptably long transient behavior. External SPI commands adjust the pulse duration.

The parallel combination of the series capacitor at the transmitter output, the capacitor used for observation, and the one parallel to the NMR probe define the resonance frequency. However, the higher the series capacitance at the output, the higher the passive amplification to the probe. A differential voltage up to 13.6 V_{pp} was measured, leading to a voltage around the probe approaching 143 V_{pp}. Such a high voltage imposes using specifically designed components on board. With the probe having a quality factor above 40, the reactance value of the inductor dominates the impedance of the RL circuit. The NMR coil having a value around 79 nH, 2.4 A_{pp} flow in the probe.

The peak power consumption of the whole transmitter attains about 2 W. With a typical duty cycle of one per mil, the average power consumption reaches 2 mW.

B. Receiver

A dedicated board was made to feed the receiver directly without exciting the NMR probe. Only the series inductors of the resonant network operate in this configuration. A balun and adequate terminations ensure the propagation of a signal without reflection. The overall current consumption of the receiver hits 11.8 mA at a voltage supply of 1.2 V, including the output buffers. An image rejection ratio (IRR) of −51.7 dB at a frequency of 120 MHz was measured. This corresponds to an amplitude imbalance of 0.02 dB and a phase imbalance of 0.27° [15]. In the higher frequency case, around 280 MHz, the amplitude (phase) imbalance reaches 0.27 dB (1.65°).

The gain of the receiver was estimated based on simulations and measurements to be 37.5 dB, with 27 dB from the LNA and 10.5 dB for the combination of the mixer and the TIA.

IV. NMR Measurements

The performance of the magnetometer ASIC was validated in two whole-body MRI scanners from Philips (3 T and 7 T). The power, the LO input, the TX excitation signal, and the two I/Q channels reach the control room outside the scanner through shielded 10-meter cables. The RF signal generators providing an input to the transmitter and the mixer are Rohde & Schwarz (R&S) SMA100A and SMA100B, respectively. An R&S RTO2024 oscilloscope acquires the quadrature signals.

The results below were acquired in the 3 T scanner. Exciting the probe to reach a 90° flip angle requires a pulse duration of 8 µs. The non-overlap time of the NOC described in subsection II-C enables us to fine-tune the excitation power. The ratio between the capacitors of the resonant network is different than the results presented in subsection III-A, leading to a passive amplification of 16.8 dB from the output of the transmitter to the probe. The current flowing in the probe is thus 1.1 A_{pp}. The chosen network leads to a better SNR compared to the maximum current case degrading the system's quality factor.

The passive amplification from the probe to the receiver input in this configuration accomplishes 17.6 dB. Figure 7 presents the free induction decay (FID) of the field probe measured in the MRI scanner without further processing. The oscilloscope samples the signals with a sampling frequency of 10 MHz. A 6th-order Butterworth bandpass filter implemented in Matlab reduces the bandwidth to 1 MHz as desired for our application. After complete relaxation, the standard deviation of the complex signal reaches 311 µV. Combining the passive

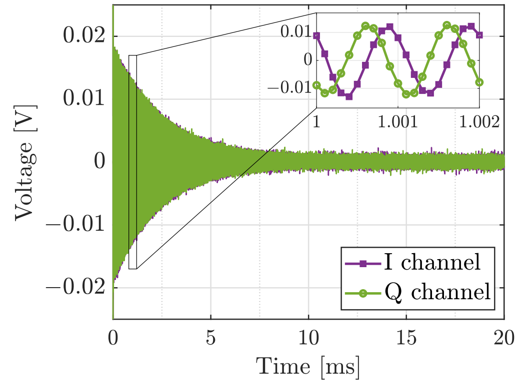

Fig. 7. Measured FID of the field probe containing Fluorine placed in the 3 T MRI scanner isocenter before any additional filtering

amplification, the receiver's gain, and the extra 3 dB coming from the quadrature signals, the total gain is equal to 58 dB. With a bandwidth of 1 MHz, the input-referred noise reaches 390 pV/$\sqrt{\text{Hz}}$.

Table I summarizes the performance of the proposed integrated transceiver for NMR field probes compared to the state-of-the-art NMR-on-a-chip transceivers. Thanks to the passive amplification at the LNA input, the proposed receiver achieves the lowest input-referred noise while being the most power efficient, as compared to the literature. The excitation voltage around the probe due to resonance is also the highest despite using a regular CMOS process.

TABLE I
Comparison to State-of-the-Art NMR-on-a-chip

	This work	F. Dreyer [7] TCAS-I'23	H. Bürkle [6] ESSCIRC'21	M. Grisi [5] Rev.Sci.Instrum.'19
Magnetic field strength [T]	3	14.1	1.13	7.05
Chip frequency range [MHz]	120–280	5–780	0.1–200	1–1000
Intermediate frequency [kHz]	1000	100	N/A	50
RX output bandwidth [kHz]	1000	250	N/A	100
Input-referred noise [nV/$\sqrt{\text{Hz}}$]	0.39	0.61	1.1	1.51[b]
RX gain [dB]	58	31.5–66	N/A	75
RX power consumption [mW]	14.2	N/A	148.5[a]	21[c]
TX output voltage [V]	3.7	2.5	50	2.5
Voltage around the probe [V_{pp}]	143	5	100	N/A
TX output current [A_{pp}]	2.4	0.21	8.3	0.028[d]
Technology [nm]	65 CMOS	130 BiCMOS	350 HV	130 CMOS
Chip area [mm^2]	1.5	1	5.8	1.8

[a]PLL included. [b]Calculated from the output noise spectral density [c]Taken from [16]
[d]Assuming current provided was RMS

V. Conclusion

This paper presented a transceiver ASIC for field probes optimized for MRI scanners. By relying on a novel resonant network structure around the transmitter and the receiver, a low-power CMOS process can be used without overlooking the performance achieved. A high excitation voltage above 140 V_{pp} around the NMR field probe was demonstrated thanks to the output network. Moreover, the passive amplification ahead of the receiver led to a low input-referred noise of 390 pV/$\sqrt{\text{Hz}}$ despite a low power consumption of 14.2 mW, making the ASIC perfectly suitable for the integration of a sensitive battery-powered magnetometer.

REFERENCES

[1] C. Barmet, N. D. Zanche, and K. P. Pruessmann, "Spatiotemporal magnetic field monitoring for MR," *Magnetic Resonance in Medicine: An Official Journal of the International Society for Magnetic Resonance in Medicine*, vol. 60, no. 1, pp. 187–197, 2008.

[2] N. De Zanche, C. Barmet, J. A. Nordmeyer-Massner, and K. P. Pruessmann, "NMR probes for measuring magnetic fields and field dynamics in MR systems," *Magnetic Resonance in Medicine: An Official Journal of the International Society for Magnetic Resonance in Medicine*, vol. 60, no. 1, pp. 176–186, 2008.

[3] J. Handwerker, M. Eschelbach, P. Chang, A. Henning, K. Scheffler, M. Ortmanns, and J. Anders, "An active TX/RX NMR probe for real-time monitoring of MRI field imperfections," in *2013 IEEE Biomedical Circuits and Systems Conference (BioCAS)*. IEEE, 2013, pp. 194–197.

[4] S. Gross, C. Barmet, B. E. Dietrich, D. O. Brunner, T. Schmid, and K. P. Pruessmann, "Dynamic nuclear magnetic resonance field sensing with part-per-trillion resolution," *Nature Communications*, vol. 7, no. 1, p. 13702, 2016.

[5] M. Grisi, G. M. Conley, P. Sommer, J. Tinembart, and G. Boero, "A single-chip integrated transceiver for high field NMR magnetometry," *Review of Scientific Instruments*, vol. 90, no. 1, 2019.

[6] H. Bürkle, T. Klotz, R. Krapf, and J. Anders, "A 0.1 MHz to 200 MHz high-voltage CMOS transceiver for portable NMR systems with a maximum output current of 2.0 App," in *ESSCIRC 2021-IEEE 47th European Solid State Circuits Conference (ESSCIRC)*. IEEE, 2021, pp. 327–330.

[7] F. Dreyer, D. Krüger, S. Baas, A. Velders, and J. Anders, "A 5–780-MHz transceiver ASIC for multinuclear NMR Spectroscopy in 0.13-μm BiCMOS," *IEEE Transactions on Circuits and Systems I: Regular Papers*, vol. 70, no. 9, pp. 3484–3496, 2023.

[8] O. Bjorkqvist and K. P. Pruessmann, "Stealth RF energy harvesting in MRI using selective shielding," *Magnetic Resonance in Medicine*, vol. 92, no. 1, pp. 406–415, 2024.

[9] G. Mocquard, O. Bjorkqvist, K. P. Pruessmann, and T. Burger, "A CMOS wireless synchronization and control system for sensor modules in MRI scanners," in *2024 IEEE Biomedical Circuits and Systems Conference (BioCAS)*, 2024, pp. 1–5.

[10] O. Bjorkqvist and K. P. Pruessmann, "Autonomous synchronization and calibration for field cameras: Book of Abstracts ESMRMB 2024 Online 40th Annual Scientific Meeting 2–5 October 2024," *Magnetic Resonance Materials in Physics, Biology and Medicine*, vol. 37, no. 1, pp. 275–276, Sep 2024. [Online]. Available: https://doi.org/10.1007/s10334-024-01191-6

[11] M. Kumngern, U. Torteanchai, and F. Khateb, "CMOS class AB second generation voltage conveyor," in *2019 IEEE International Circuits and Systems Symposium (ICSyS)*. IEEE, 2019, pp. 1–4.

[12] J. F. da Rocha, M. B. dos Santos, J. M. D. Costa, and F. A. Lima, "Level shifters and DCVSL for a low-voltage CMOS 4.2-V buck converter," *IEEE Transactions on Industrial Electronics*, vol. 55, no. 9, pp. 3315–3323, 2008.

[13] B. J. Thijssen, E. A. Klumperink, P. Quinlan, and B. Nauta, "2.4-GHz highly selective IoT receiver front end with power optimized LNTA, frequency divider, and baseband analog FIR filter," *IEEE Journal of Solid-State Circuits*, vol. 56, no. 7, pp. 2007–2017, 2020.

[14] G. Mitteregger, C. Ebner, S. Mechnig, T. Blon, C. Holuigue, and E. Romani, "A 20-mW 640-MHz CMOS continuous-time $\Sigma\Delta$ ADC with 20-MHz signal bandwidth, 80-dB dynamic range and 12-bit ENOB," *IEEE Journal of Solid-State Circuits*, vol. 41, no. 12, pp. 2641–2649, 2006.

[15] J. K. Cavers and M. W. Liao, "Adaptive compensation for imbalance and offset losses in direct conversion transceivers," *IEEE Transactions on Vehicular Technology*, vol. 42, no. 4, pp. 581–588, 1993.

[16] M. Grisi, G. Gualco, and G. Boero, "A broadband single-chip transceiver for multi-nuclear NMR probes," *Review of Scientific Instruments*, vol. 86, no. 4, 2015.